Petroleum Science 23 (2026) 1402–1415

Contents lists available at ScienceDirect

Petroleum Science

journal homepage: www.keaipublishing.com/en/journals/petroleum-science

Original Paper

Double-crosslinked self-degradable hydrogel for temporary plugging in low temperature reservoirs

Tai-Heng Yin [a,1], Yu-Meng Zhu [a,1], Yu-Qi Yang [a,*], Shen-Gen Chen [b], Ji-Rui Chen [a], Yuan-Yuan Lu [c], Han-Yu Guo [a], Tao Wan [a], Jian Liu [a]

[a] China University of Petroleum–Beijing at Karamay, Karamay, 834000, Xinjiang, China
[b] Production Technology Research Institute, PetroChina Xinjiang Oilfield Company, Karamay, 834000, Xinjiang, China
[c] Sichuan College of Architectural Technology, Deyang, 618000, Sichuan, China

ARTICLE INFO

Article history:
Received 2 June 2025
Received in revised form
7 November 2025
Accepted 11 November 2025
Available online 15 November 2025

Edited by Yan-Hua Sun

Keywords:
Self-degradable
Double-crosslinked hydrogel
Polydopamine
Low temperature reservoir
Temporary plugging agent

ABSTRACT

Temporary plugging agents are critical to oilfield operations such as diversion fracturing, wellbore interventions, and drilling. This study develops a double-crosslinked self-degradable gel (DSDG) using polydopamine and poly(ethylene glycol) diacrylate as crosslinkers for polyacrylamide, targeting low temperature reservoirs. The DSDG system integrates covalent crosslinking via C=C bonds and dynamic crosslinking through amine–catechol interactions. Gelation kinetics, rheological properties, self-degradation mechanisms, and gel breaking performance of DSDG were systematically characterized. By analyzing the influence of components on gelation kinetics and mechanical properties, the composition of DSDG was optimized to include 4–8 wt% acrylamide monomer, 0.5–0.8 wt% initiator, and 0.2–0.6 wt% poly(ethylene glycol) diacrylate crosslinker, with a dopamine to acrylamide mass ratio of (5–8) × 10^{-3}. At 60–80 °C, DSDG transitions from liquid to quasi-solid gel within 30–180 min, with > 80% of the gelation process occurring in a low viscosity phase conducive to pumpable injection. Unoxidized catechol groups, π–π stacking, and hydrogen bonding synergistically enhance tensile strength, fracture toughness, and interfacial adhesion, enabling robust sealing under downhole stresses. Core flooding tests in 5–50 mD cores achieved initiation and breakthrough pressure gradients of 34.6–119 and 86.6–184.6 MPa/m, respectively. In simulated wellbore with an inner diameter of 120 mm, the pressure-bearing capacity reached 1.25 MPa/m. Acidic/alkaline conditions rapidly degrade polydopamine, disrupting network integrity and enabling controllable gel breaking times of 1–20 d. Free dopamine monomers inhibit acrylamide polymerization, reducing post-degradation viscosity to < 10 mPa·s via shortened polyacrylamide chains.

1. Introduction

Temporary plugging technology plays a crucial role in oil and gas development engineering fields such as refracturing, downhole operations, and pressure-controlled drilling. As a critical component of reservoir stimulation strategies, effective temporary plugging enables the creation of new fracture networks while reactivating under-depleted existing fractures, thereby improving productivity in unconventional reservoirs (Li et al., 2024; Liu et al., 2021; Zhong et al., 2022). For well intervention applications, this technology addresses downhole failures with precision, increasing single-well production rates and ultimate recovery while extending operational lifespans (Jia et al., 2019, 2020; Zhong et al., 2022). In drilling engineering, temporary plugging agents mitigate fluid loss by sealing formation channels, preventing drilling mud invasion into pay zones (Bai et al., 2023; Du et al., 2023; Li et al., 2024).

Recent years have witnessed a gradual transition in temporary plugging technologies within oil and gas fields from traditional mechanical methods to chemical approaches characterized by operational simplicity, enhanced safety, and superior efficiency (Yang et al., 2024; Zhao and Bai, 2022; Zhou et al., 2025). This

* Corresponding author.
E-mail address: yuqiyang@cupk.edu.cn (Y.-Q. Yang).
Peer review under the responsibility of China University of Petroleum (Beijing).
[1] These authors contributed equally to this work.

https://doi.org/10.1016/j.petsci.2025.11.025

evolution has driven the development of diverse functional chemical temporary plugging agents tailored for specific operational needs (He et al., 2021). Among these, gel-based temporary plugging agents, defined as materials capable of forming gel-like blocking layers under predetermined conditions to temporarily seal fractures and pores in wellbores or formations, have attracted significant attention (Bai et al., 2022). These agents are categorized into self-degrading systems and those requiring external breakers based on their degradation mechanisms (Khan et al., 2019). In this study, self-degradable refers to a hydrogel that, without any external breaker or mechanical disruption, undergoes spontaneous disintegration under in-situ reservoir conditions (specific temperature, pH, or redox environment) due to intrinsic chemical instability of its crosslinks or internal reactive moieties. Self-degrading gels, which autonomously form and disintegrate within formations, offer distinct advantages over conventional methods involving post-injection of degradation agents or premixed encapsulated breakers, including residue-free degradation and precise temporal control, thereby garnering substantial research interest (Bai et al., 2022). However, existing systems face critical limitations in low temperature reservoirs (< 90 °C). For example, Zhang et al. (2022) developed degradable gel particles that achieve complete degradation within 19–107 h at 100–160 °C, yet their degradation efficiency markedly decreases below 80 °C, accompanied by poor injectivity due to particle agglomeration in heterogeneous fractures. Wang et al. (2022) formulated a high-strength liquid temporary plugging agent using acrylamide (AM), acrylic acid (AA), and an unstable cross-linking agent (SEG), neopentyl glycol diacrylate. The agent exhibited compatibility with low temperature reservoirs and a degradation time of 180–300 h. Nevertheless, this system requires excessively high AM monomer concentrations (> 8 wt%), exhibits prolonged SEG degradation periods, suffers from rapid gelation rates, and generates post-degradation fluids with elevated viscosity (> 50 mPa·s), all of which impair injection and flowback performance. The incorporation of AA further exacerbates these issues by increasing the loss modulus (G''), leading to gel deformation under operational stresses and subsequent reductions in pressure-bearing capacity. Ji et al. (2024) designed a self-degrading temporary valve for managed pressure drilling that degrades within 5–20 d at 90 °C. While demonstrating favorable injectivity, this system shows significantly prolonged degradation cycles below 80 °C and limited tunability spanning only 15 d, restricting its applicability. A comprehensive analysis indicates that current research on temporary plugging agents predominantly focuses on high temperature reservoirs of > 90 °C, while specialized formulations for low temperature reservoirs remain relatively underdeveloped. Existing temporary plugging agents for low temperature applications universally face technical bottlenecks such as excessively rapid gelation rates within 30 min. Furthermore, the degradation timelines of available products exhibit a polarized distribution spanning 1–7 or 7–15 d, resulting in incompatibility between specialized agents for different operational scenarios such as fracturing temporary plugging and wellbore temporary plugging. Therefore, it is imperative to develop a novel self-degrading gel temporary plugging agent suitable for low temperature reservoirs with broad tunability in gelation and degradation times, easy injectivity, and low post-degradation viscosity (Jia et al., 2022, 2024).

Gels are three-dimensional network structures composed of polymer chains and crosslinking points. Current self-degrading hydrogels are primarily prepared using unstable crosslinkers such as poly(ethylene glycol) diacrylate (PEGDA) and SEG, where the degradation of these crosslinkers disrupts the gel network by breaking crosslinking points. However, such crosslinkers still exhibit prolonged degradation times under low temperature conditions. Although methods like adding AA, polylactic acid can shorten degradation times, they introduce persistent issues including high monomer concentrations, low gel strength, excessively rapid gelation rates, poor degradation controllability, and narrow operational windows (Liu et al., 2024; Zou et al., 2023). In recent years, bioinspired materials have opened new avenues for hydrogel design. Polydopamine (PDA), a synthetic analog of mussel adhesive proteins, has garnered attention for its unique combination of catechol-rich chemistry, redox activity, and pH-responsive degradation (Deng et al., 2018). The catechol moieties in PDA enable dynamic noncovalent interactions, such as hydrogen bonding, π–π stacking, and metal coordination, that enhance mechanical strength and interfacial adhesion at low monomer concentrations (Du et al., 2022; Guo et al., 2022). Han et al. (2017) demonstrated that incorporating merely a DA/AM mass ratio of $(2–8) \times 10^{-3}$ in hydrogels significantly improved tensile strength and fracture toughness while enabling self-healing properties. Critically, the inherent redox activity of PDA prolongs gelation time by suppressing free radical polymerization via scavenging of initiator-derived radicals. Concurrently, catechol groups in PDA crosslink with amine groups in polyacrylamide (PAM) through Michael addition and Schiff base reactions, while enabling the incorporation of supplementary crosslinkers to establish stable double-crosslinked structures (Xu et al., 2023). For example, PDA has been employed as a dynamic covalent crosslinking agent bridging cellulose and PAM, enabling the synthesis of a cellulose based double-crosslinked hydrogel via single step solution polymerization (Li et al., 2018). Notably, the reducibility of PDA suppresses crosslinking reactions of other crosslinkers, reducing its proportion of crosslinking points within the gel network (Zhang et al., 2020). Owing to the pH-sensitivity of PDA, it degrades under both acidic and alkaline conditions (Wu et al., 2023). When PDA participating in gel network crosslinking degrades, the structural integrity of the gel network is inevitably compromised (Chen et al., 2021). In summary, PDA can form double-crosslinked structures with other crosslinkers to enhance mechanical performance. The reducibility of PDA-mediated inhibition of free radical polymerization prolongs gelation time, while its effects including shortened polymer chains, suppression of other crosslinking reactions, and post-degradation network disruption collectively accelerate degradation. Therefore, incorporating self-degradable PDA crosslinkers into traditional AM gel systems may simultaneously enhance gel strength and broaden the degradation time regulation range.

This study developed a double-crosslinked self-degradable gel as a temporary plugging agent for low temperature reservoirs. The composite hydrogel is synthesized via free radical polymerization, achieving enhanced mechanical properties at reduced monomer concentrations. By leveraging the high density catechol functional groups on PDA surfaces and incorporating the thermally unstable crosslinker PEGDA, a double-crosslinked network is constructed. The pH responsive degradation of PDA disrupts the structural integrity of the gel network under acidic or alkaline conditions, addressing the limitations of conventional ester based crosslinked systems, such as uncontrollable degradation initiation, narrow adjustment windows, and insufficient gel strength. The strong reducibility of free hydrochloride dopamine (DA) monomers inhibits AM polymerization, prolonging gelation time while reducing post-degradation solution viscosity through shortened PAM chain lengths (Zhang et al., 2020). A systematic investigation of gelation kinetics, rheological performance, pressure bearing capacity, self-degradation mechanisms, and flowback behavior was conducted to optimize the DSDG formulation. The synergistic mechanism between in-situ gelation and autonomous

degradation was elucidated, driven by the interplay of PDA-mediated covalent crosslinking and PEGDA ester bond hydrolysis. Fig. 1 illustrates the preparation process and degradation mechanisms. DSDG was synthesized via a straightforward two-step procedure. Initially, DA underwent oxidative polymerization in an alkaline oxygen-rich environment to form PDA nanoparticles. Subsequently, AM was polymerized and cross-linked with both PDA and PEGDA to establish a three-dimensional polymer network. The catechol groups on PDA were oxidized to *o*-quinone, which exhibits high reactivity. These active groups can further react with the amino groups of PAM through Michael addition or Schiff base reactions to form covalent bonds (Liu and Huang, 2016). Additionally, the phenol groups on PDA and the carbonyl groups on PAM can form hydrogen bonds with amino groups, providing non-covalent interactions (Chen et al., 2017; Peng et al., 2023). This results in a crosslinked and dual-network structure between PDA and PAM chains. The hydrogel undergoes two sequential and internally driven reactions without external breakers. First, PDA nanoparticles are oxidized and cleave into small dopamine-derived fragments, thereby losing their effectiveness as a particulate crosslinker. Then, PEGDA ester hydrolysis takes place whereby the ester bonds in PEGDA are progressively hydrolyzed under thermal or pH conditions, resulting in the breaking of covalent crosslinks. The synergistic action of these two intrinsic reactions causes autonomous loss of mechanical integrity and eventual dissolution of the network (Lin et al., 2015; Zhou M. et al., 2025).

2. Experimental section

2.1. Materials

DA, AM, potassium persulfate (KPS), PEGDA (average molecular weight 170.16), sodium hydroxide (NaOH), and dilute hydrochloric acid (0.1 mol/L) were of reagent grade and used as received. All chemicals were obtained from Shanghai Macklin Biochemical Technology Co., Ltd. (Shanghai, China). Deionized water was used for all solution preparations.

2.2. DSDG preparation

DA was added to a beaker containing NaOH aqueous solution (pH 11) and fully dissolved. The solution was stirred under an air atmosphere for 20 min to allow the oxidative polymerization of DA into PDA nanoparticles. Simultaneously, PDA nanoparticle size was modulated by stirring duration, with longer stirring times resulting in larger PDA particle sizes. The mixture of AM, KPS, PEGDA, and PDA solution was then mixed under nitrogen protection with stirring. After 10 min of homogenization, dilute hydrochloric acid was added dropwise to adjust the solution pH to 3–11. Approximately 15 mL of the prepared gel solution was transferred into glass centrifuge tubes, while 80 mL was injected into blue-capped glass bottles, followed by nitrogen purging and sealing. The containers were stored in a thermostatic oven at 60–100 °C to observe gelation and degradation behavior. Notably, excess KPS was required to compensate for radical consumption by DA during secondary polymerization. All experiments were conducted at 80 °C unless otherwise specified.

2.3. Determination of the gelation time and degradation time

The gelation time and gel strength were determined using the gel strength code method (Mandal et al., 2024). This method involves inverting the glass centrifuge tubes and observing the flow state of the gel to rapidly assess its strength, enabling classification across a broad spectrum of gel strength. During the experiment, the glass centrifuge tubes were slowly inverted by 180° at 5-min intervals, and the gel strength was recorded. The gel strength was graded according to codes A to I (Fig. 2), with the time required for the gel strength to progress from code A to code I defined as the gelation time. For field applications, a gel strength reduction to code C is sufficient to restore operational flow.

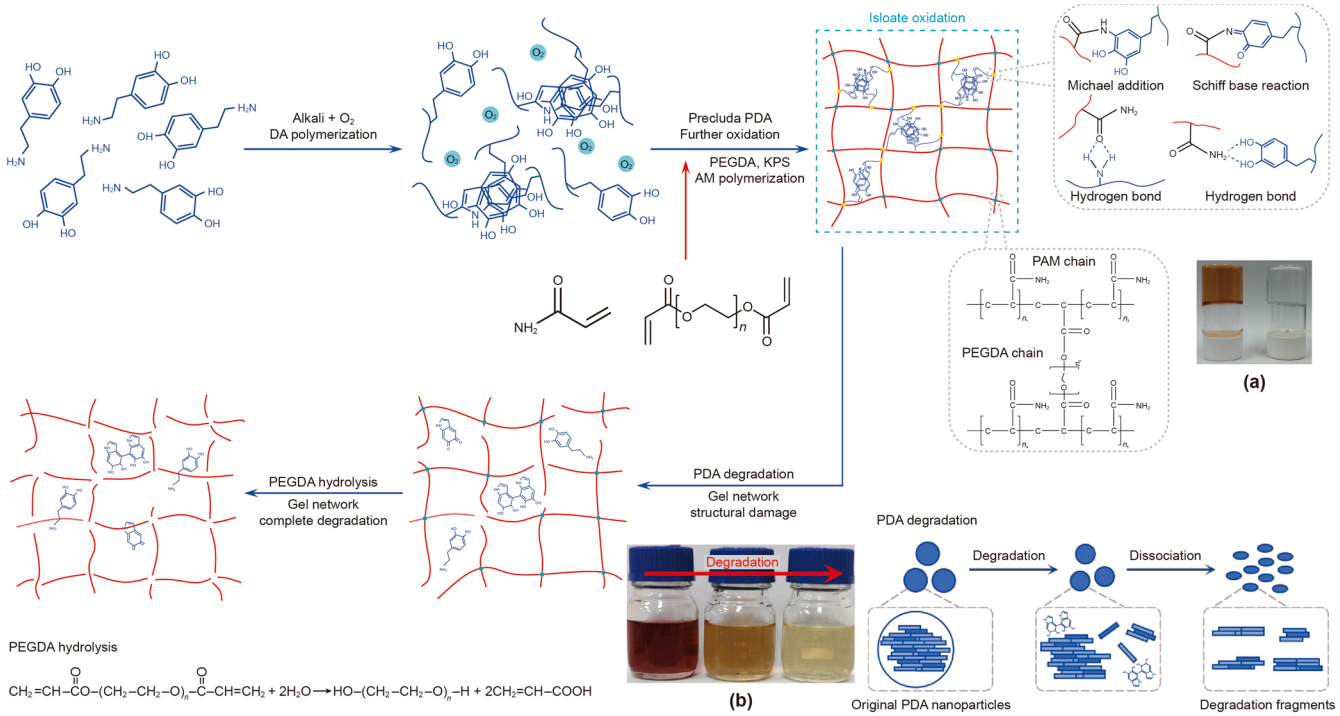

Fig. 1. Schematic diagram of gel cross-linking and degradation: (**a**) DSDG (left) and PAM-PEGDA (right), (**b**) the degradation of PDA solution at 80 °C.

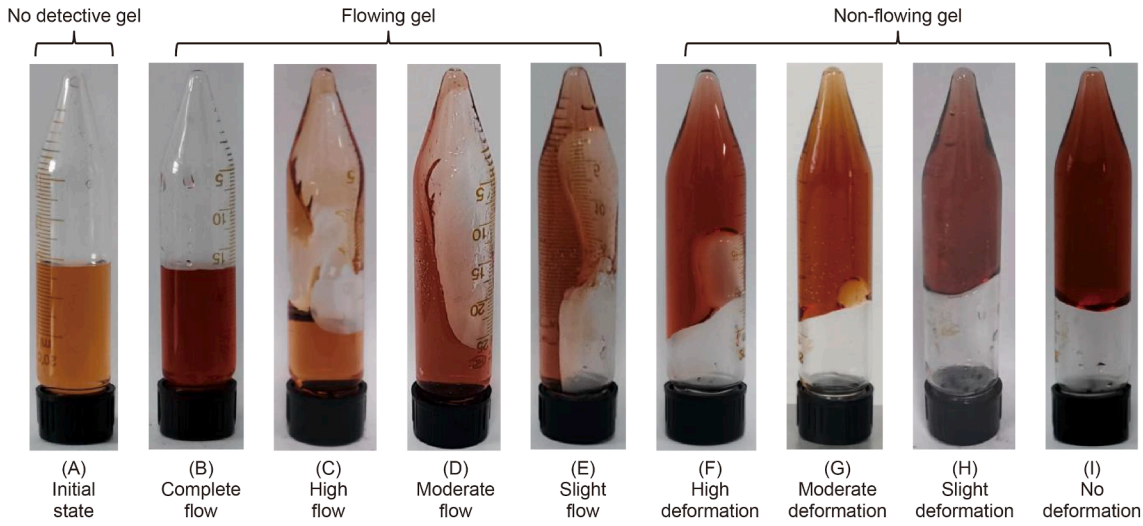

Fig. 2. Schematic diagram of different gel strength.

Therefore, the degradation time was defined as the duration required for the fully formed gel to decline from its maximum strength to code C. This parameter was determined by continuously monitoring the flow behavior of the gel within blue-capped glass bottles under controlled temperature conditions.

2.4. Rheological measurement

The rheological properties of DSDG were measured using a rotational rheometer (HAAKE MARS iQ, Thermo Fisher Scientific, Germany) with a P35/Ti/SE rotor. The gel sample was placed on the measurement platform, and viscosity changes during gelation were recorded under controlled shear rates. Additionally, the linear viscoelastic region of the DSDG was determined under oscillatory conditions at a fixed frequency of 1.0 Hz and strain range of 1.0%–150%. Subsequent frequency sweep tests from 0.01 to 10 Hz were conducted to measure the storage modulus (G') and loss modulus (G''). The viscosity of post-degradation fluid was measured using a Brookfield viscometer. All experiments were performed at 80 °C.

2.5. Scanning electron microscopy (SEM)

The gel samples were sectioned into small pieces and placed on quartz plates for freeze-drying. The nanoparticles were washed three times with deionized water and ethanol to remove residual reactants and then dried in a constant-temperature oven at 60 °C. The processed gel and nanoparticle samples were imaged using a HITACHI SU8010 field-emission scanning electron microscope to observe their micromorphology.

2.6. Fourier-transform infrared (FTIR) spectroscopy

FTIR spectra of pure PDA nanoparticles, pure PAM hydrogel, and the DSDG were recorded using an FTIR spectrometer (FTIR-850, ANDONG, China) at room temperature. Spectra were collected in the wavenumber range of 500–4000 cm^{-1} to identify characteristic functional groups and chemical interactions. Prior to measurement, pure PDA nanoparticle samples were washed three times with deionized water and ethanol to remove residual reactants and dried in a constant-temperature oven at 60 °C. Hydrogel samples were freeze-dried at −50 °C for one week.

2.7. Gel temporary plugging performance test

The pressure-bearing capacity of the DSDG was evaluated in simulated wellbores and homogeneous sandstone cores using a custom experimental setup shown in Fig. 3, consisting of an N_2 pressure supply system, plunger pump, thermostatic oven, pressure signal acquisition system, core holder, and N80 steel wellbore model with 120 mm inner diameter. The wellbore interior was coated to eliminate corrosion effects on gel performance. For wellbore tests, the gel solution was aged at 80 °C for 6 h, followed by continuous N_2 injection at the bottom until a sudden pressure drop occurred, the pressure from the preceding stage was recorded as the maximum bearing pressure (Wang et al., 2022). Core flooding experiments utilized artificial sandstone cores with physical parameters listed in Table 1. The procedure began with water injection to stabilize baseline pressure, followed by injection of 2 pore volumes (PV) of DSDG solution. After 5 h of gelation at 80 °C, post-gelation waterflooding was performed until pressure stabilization. Post-degradation waterflooding was conducted after aging the gel-filled cores at 80 °C until complete degradation. To simulate in-situ gelation, plugging, and degradation performance, the core was maintained in the core holder under simulated reservoir conditions throughout the experiment. Plugging efficiency and formation damage were assessed by comparing pre-gelation, post-gelation, and post-degradation waterflooding pressures (Zhu et al., 2018, 2019).

3. Results and discussion

3.1. Gelation performances

3.1.1. Influence of monomer concentration

The gelation behavior of the DSDG was investigated under varying AM monomer concentrations ranging from 2.0 to 7.0 wt% at 80 °C and pH 11, with fixed initiator concentration of KPS at 0.6 wt%, PEGDA crosslinker at 0.4 wt%, and a DA/AM mass ratio of 5×10^{-3}. Fig. 4 illustrates the influence of monomer concentration on gelation time, demonstrating that the gelation time of DSDG decreases with increasing monomer concentration. At monomer concentrations below 3.0 wt%, the hydrogel failed to form a stable network, exhibiting insufficient strength for field applications. Optimal performance was observed at 4.0–6.0 wt% AM, achieving code I gel strength within 30–55 min while maintaining

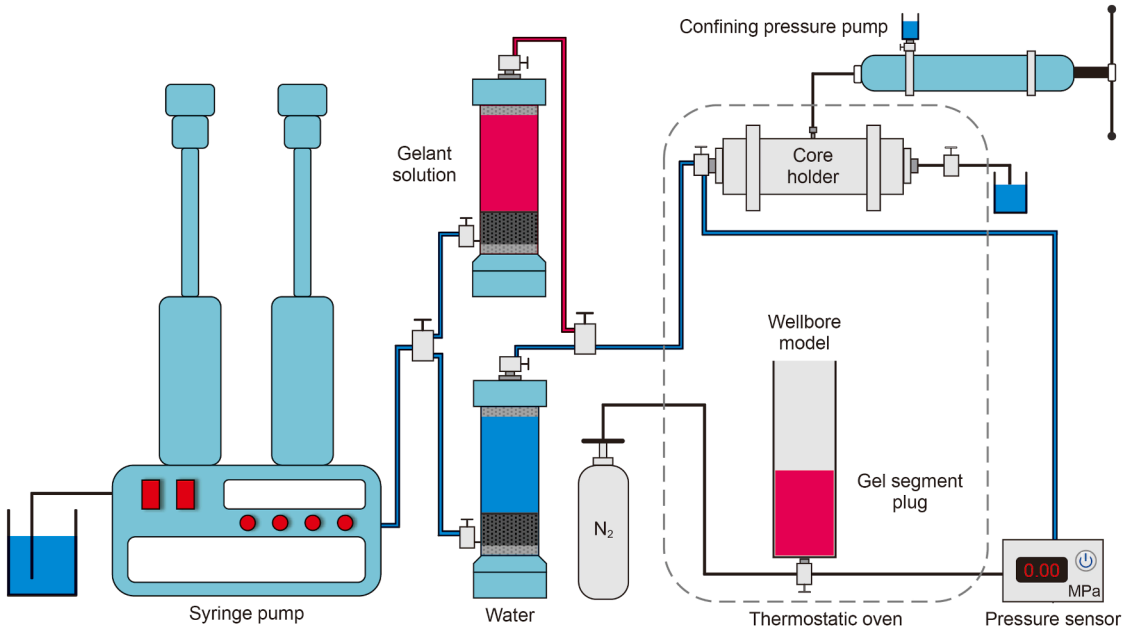

Fig. 3. Schematic diagram of gel pressure resistance testing device.

Table 1
Physical parameters of artificial sandstone core.

Number	Length, mm	Diameter, mm	Porosity, %	Permeability, mD
1	50.26	38.33	10.23	4.97
2	50.07	38.33	15.61	10.85
3	50.25	38.08	23.25	49.72
4	50.15	38.28	15.35	9.91
5	50.12	38.27	14.86	11.01
6	50.34	38.32	15.08	9.76
7	50.32	38.16	15.24	10.42

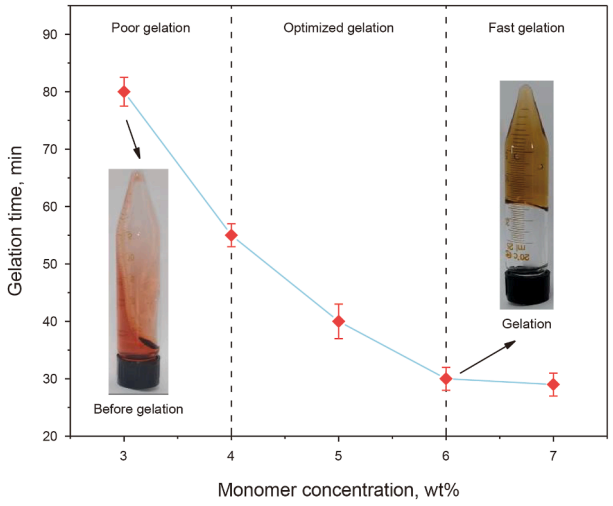

Fig. 4. Gelation performance of the DSDG prepared with different monomer concentrations.

pumpability. Concentrations exceeding 7.0 wt% resulted in excessively rapid gelation (< 30 min), posing risks of premature plugging in near-wellbore zones. These findings demonstrate that monomer concentration critically governs both gelation kinetics and mechanical robustness, necessitating precise formulation control for operational reliability.

3.1.2. *Influence of initiator concentration*

The effect of initiator (KPS) concentration on the gelation time of DSDG was investigated under fixed conditions including 5 wt% AM monomer, 0.4 wt% PEGDA crosslinker, and a DA/AM ratio of 5×10^{-3}, pH 11, and 80 °C. Gelation time decreased with increasing initiator concentration, as shown in Fig. 5. However, the rate of reduction slowed significantly above 0.6 wt% initiator, indicating saturation of free radical availability for polymerization. Below 0.5 wt% initiator, insufficient radical generation led to incomplete gel formation due to the radical scavenging effects of DA (Han et al., 2017). Optimal initiator concentrations ranging from 0.5 to 0.8 wt% balanced gelation kinetics of 52–82 min with mechanical stability, ensuring sufficient time for downhole placement while achieving code I gel strength. These findings underscore the necessity of precise initiator dosage to counteract the inhibition by

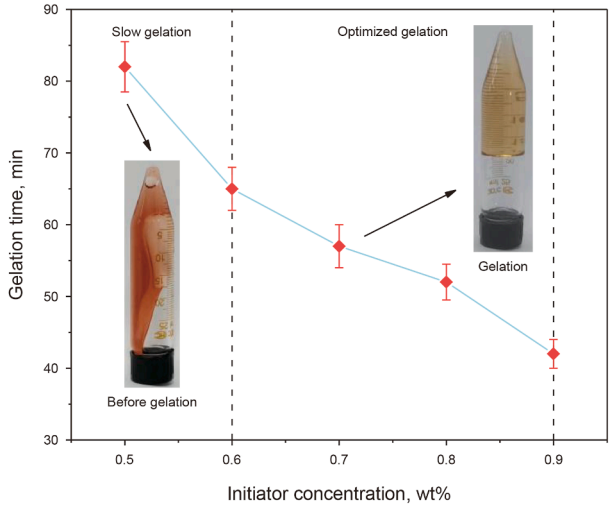

Fig. 5. Gelation performance of the DSDG prepared with different initiator concentrations.

DA and regulate polymerization rates in double-crosslinked systems.

3.1.3. Influence of DA/AM mass ratio

The effect of DA/AM mass ratio on gelation time was studied under fixed conditions including 5 wt% AM monomer, 0.4 wt% PEGDA crosslinker, 0.6 wt% KPS initiator, pH 11, and 80 °C. As shown in Fig. 6, gelation time increased with higher DA/AM mass ratios due to the radical scavenging effect of free DA monomers, which suppressed AM polymerization. At DA/AM mass ratios exceeding 10×10^{-3}, excessive unreacted DA monomers destabilized the crosslinking process, resulting in incomplete network formation (Li et al., 2022). Optimal performance was achieved at DA/AM mass ratios of $(5–9) \times 10^{-3}$, balancing prolonged gelation time with sufficient mechanical strength (code I). These results demonstrate that DA/AM mass ratio critically regulates gelation kinetics, providing a tunable parameter for field-specific applications.

3.1.4. Influence of PDA particle size

The gelation behavior of DSDG was investigated as a function of PDA particle size ranging from 110 to 340 nm (Fig. S1), controlled by varying the pre-polymerization duration of DA monomers. Experiments were conducted at 80 °C and pH 11 under fixed conditions including 5 wt% AM monomer, 0.4 wt% PEGDA crosslinker, 0.6 wt% KPS initiator, and a DA/AM mass ratio of 8×10^{-3}. As shown in Fig. 7, gelation time increased with PDA particle size within the 110–270 nm range, attributed to the reduced surface density of reactive catechol groups per unit mass. Beyond 270 nm, prolonged pre-polymerization diminished the concentration of free DA monomers and unoxidized catechol groups, leading to shorter gelation times despite larger particle sizes. The depletion of unoxidized catechol groups during extended pre-polymerization adversely affected both interfacial adhesion and crosslinking density, critical for maintaining plugging efficiency. These results reveal a dual dependency: smaller PDA particles enhance reaction efficiency through higher surface activity, while excessive pre-polymerization sacrifices functional group availability. Optimal performance was achieved with PDA particle sizes of 110–270 nm, balancing gelation kinetics with mechanical robustness for practical applications.

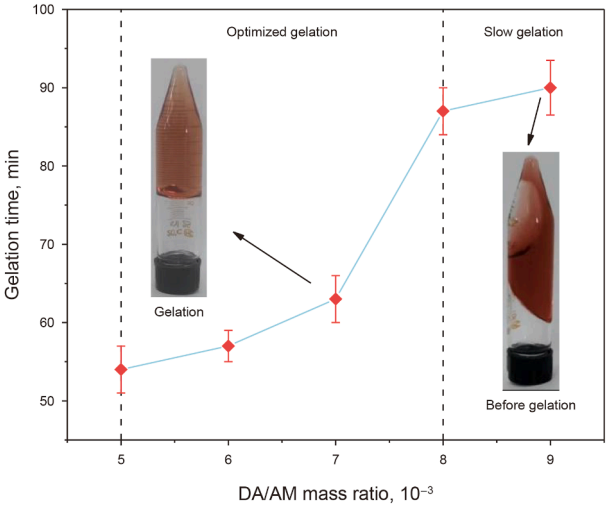

Fig. 6. Gelation performance of the DSDG prepared with different DA/AM mass ratios.

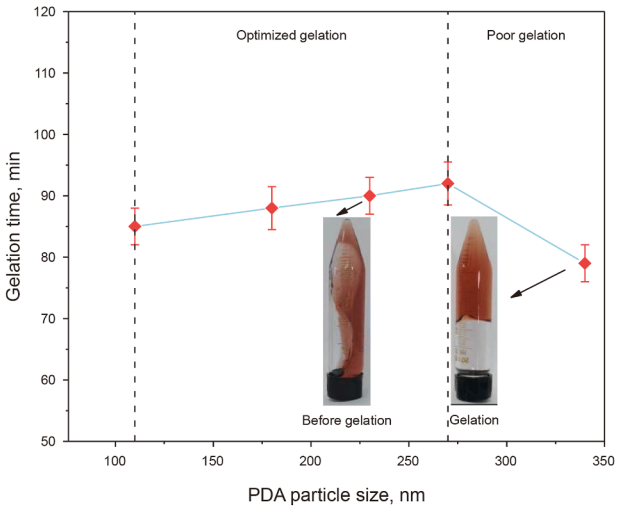

Fig. 7. Gelation performance of the DSDG prepared with different PDA particle sizes.

3.1.5. Influence of crosslinker PEGDA concentration

The effect of PEGDA crosslinker concentration on gelation behavior was evaluated at 80 °C and pH 11, with fixed parameters including 5 wt% AM monomer, 0.6 wt% KPS initiator, and a DA/AM mass ratio of 8×10^{-3}. As shown in Fig. 8, gelation time decreased with increasing PEGDA concentration due to the higher density of reactive acrylate groups available for covalent crosslinking. At PEGDA concentrations below 0.2 wt%, prolonged gelation allowed significant alkaline degradation of PDA, severely compromising mechanical strength and interfacial adhesion. The double-crosslinked architecture, combining PDA pH-sensitive covalent bonds and PEGDA thermally labile ester linkages, mitigated the limitations of single-crosslinker systems. Optimal performance was achieved at PEGDA concentrations of 0.3–0.6 wt%, while ensuring structural stability and preventing excessive rapid formation of the gel network.

3.1.6. Influence of pH

The gelation time of DSDG was evaluated across a pH range of 3–11 at 80 °C under fixed conditions including 5 wt% AM monomer, 0.4 wt% PEGDA crosslinker, 0.6 wt% KPS initiator, and a DA/

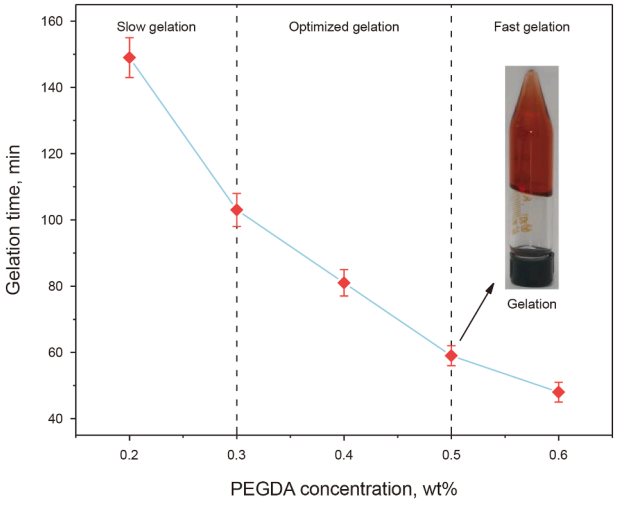

Fig. 8. Gelation performance of the DSDG prepared with different PEGDA concentrations.

AM mass ratio of 8 × 10^{-3}. As shown in Fig. 9, gelation time increased with alkalinity in the pH 7–11 range, attributed to accelerated PDA self-polymerization that consumed free radicals and suppressed AM polymerization. Under acidic conditions, protonation of AM amino groups (–NH_2 to –NH_3^+) hindered polymerization kinetics, thereby extending gelation time. These results demonstrate that gelation kinetics can be precisely modulated by adjusting solution pH within the 3–11 range, providing operational flexibility for field-specific requirements.

3.1.7. Influence of temperature

The gelation behavior of DSDG was investigated across a temperature range of 60–100 °C under fixed conditions including 5 wt% AM monomer, 0.4 wt% PEGDA crosslinker, 0.6 wt% KPS initiator, pH 11, and a DA/AM mass ratio of 8 × 10^{-3}. As shown in Fig. 10, gelation time decreased progressively with increasing temperature within the 60–100 °C range. At temperatures below 60 °C, insufficient thermal energy prevented KPS decomposition, resulting in failed gelation. The temperature-dependent decomposition of KPS governed free radical generation rates, directly influencing AM polymerization kinetics. Higher temperatures accelerated initiator breakdown, increasing radical concentration and shortening gelation time. However, excessively rapid polymerization at elevated temperatures > 90 °C risked premature viscosity buildup, complicating downhole placement. Optimal performance was achieved between 60 and 80 °C, balancing controllable gelation times with operational feasibility. These results demonstrate that temperature serves as a critical lever for tuning gelation kinetics in double-crosslinked systems, enabling adaptation to diverse reservoir conditions.

3.2. Rheological properties

Rheological properties of the DSDG were characterized using a rheometer, including viscosity evolution during gelation and degradation, as well as G' and G''. Fig. 11 illustrates the viscosity variation of DSDG during gelation at 80 °C. Within the initial 0–4000 s, the viscosity of the DSDG solution remained stable, attributed to the early stage of free radical polymerization where high monomer content and low polymer molecular weight minimized viscosity changes. Between 4000 and 4200 s, gradual viscosity increase occurred due to polymer chain growth and localized chain aggregation. From 4200 to 5000 s, rapid viscosity

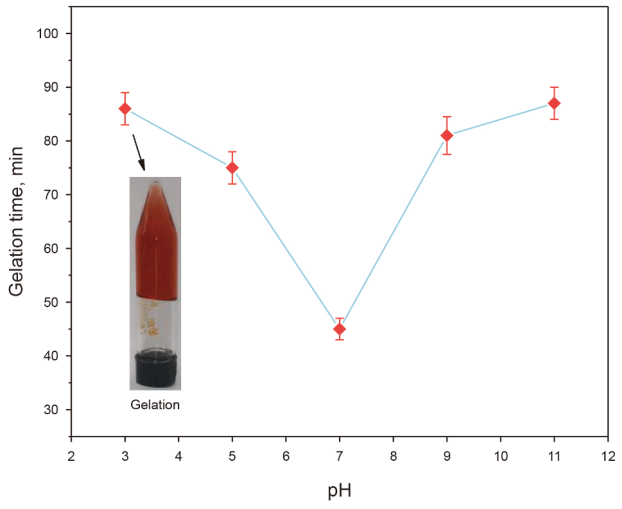

Fig. 9. Gelation performance of the DSDG prepared with different pH.

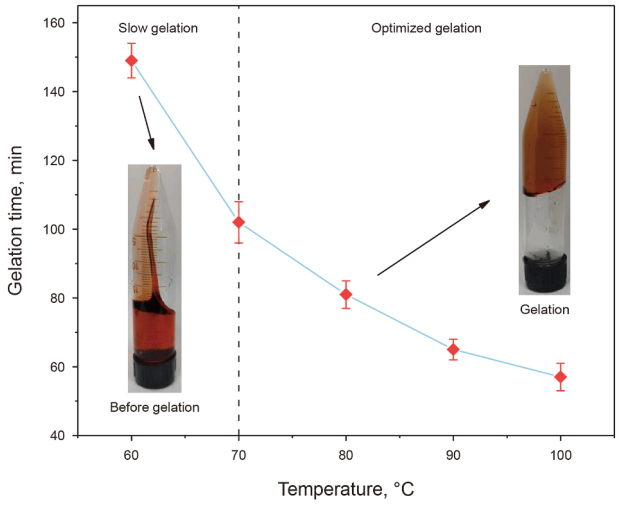

Fig. 10. Gelation performance of the DSDG prepared with different temperature.

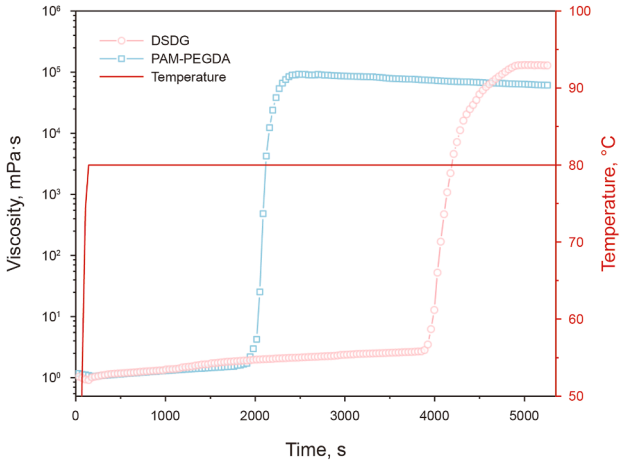

Fig. 11. Viscosity variation of the DSDG solution during the gelation process.

escalation marked the formation of a three-dimensional network through progressive crosslinking. Experimental results demonstrate that DSDG maintained low viscosity for over 80% of the total gelation time, ensuring injectability for field operations. Post-gelation viscosity reached 1.31 × 10^5 mPa·s, confirming effective sealing in formation/wellbore environments. In contrast, PDA-free gels exhibited premature viscosity rise at 2000 s, followed by rapid escalation after 2100 s. The low-viscosity duration of the control system was only 50% of DSDG, with a final viscosity reaching merely 70% of DSDG. This highlights the inferior injectability and plugging efficacy of conventional PAM-PEGDA gels.

Subsequently, the viscoelastic properties of the hydrogel were assessed by measuring the G' and G'' across a frequency range of 0.01–10 Hz, with particular focus on the effects of monomer concentration and DA/AM mass ratio. Gel solutions were injected into blue-capped glass bottles, purged with nitrogen, and cured at 80 °C until reaching code I gel strength, followed by 5 h of additional thermal stabilization to ensure sample consistency. Fig. 12 demonstrates the influence of AM monomer concentration on the viscoelastic moduli. Both G' and G'' increased with higher AM concentrations, attributable to elevated polymer chain molecular weights and enhanced crosslinking density. These factors strengthened intermolecular interactions and network constraints, enabling improved structural retention under

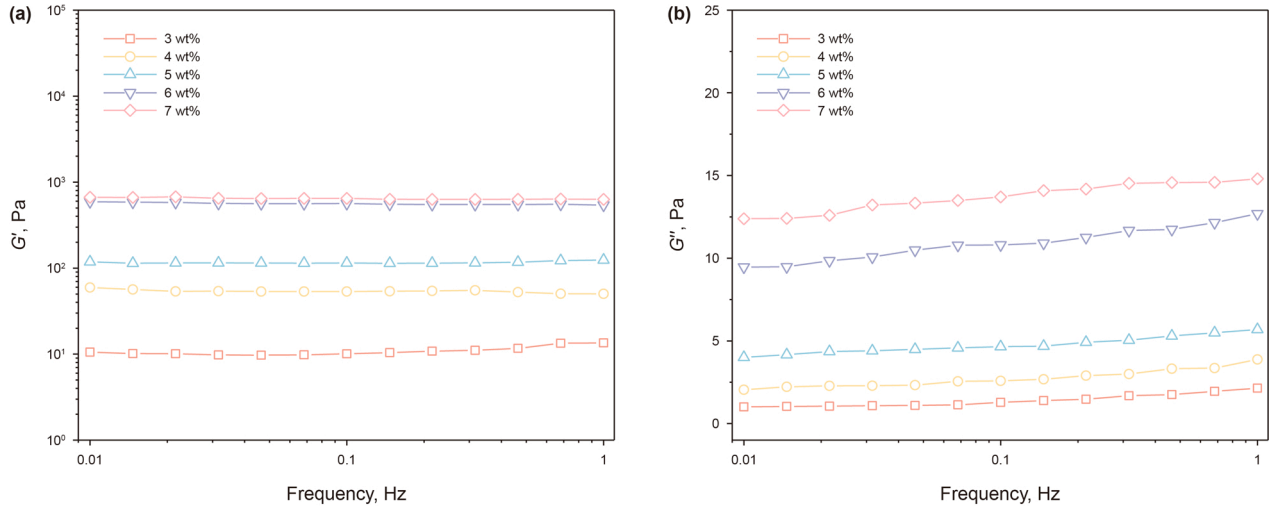

Fig. 12. G' (**a**) and G'' (**b**) of the prepared DSDG with different monomer concentrations.

external stresses. The concurrent rises in G' and G'' reflect the dual impact of chain entanglement and crosslink-driven network stiffening.

Fig. 13 illustrates the effect of DA/AM mass ratio on rheological behavior. Increasing PDA concentration augmented G' and G'' through covalent crosslinking between PDA catechol groups and PAM amino groups, forming a denser three-dimensional network. PDA π–π stacking and hydrogen bonding introduced reversible non-covalent interactions that dissipated energy during deformation, inhibiting crack propagation and enhancing toughness. Furthermore, the synergy between covalent and non-covalent crosslinks enabled stress distribution across the network, improving overall elasticity. At DA/AM mass ratios exceeding 7×10^{-3}, excessive free DA monomers intensified radical scavenging, suppressing crosslinking density and network integrity. The inherent flexibility and reversibility of hydrogen bonds further promoted elastic deformation under stress, resulting in reduced G' and G''.

The enhancement of G' improves the elasticity of the hydrogel, enabling resistance to deformation under external forces, but reduces gel flexibility. Excessively high G' may render the gel prone to fracture under high pressure. Elevated G'' enhances flexibility and ductility, mitigating fracture risks under high-pressure conditions; however, gels with excessively high G'' are susceptible to deformation during operational use. In contrast, gels with low G'' maintain network stability, preserving structural integrity under mechanical stress. Both fracture and excessive deformation adversely affect plugging efficacy. As demonstrated in Figs. 12 and 13, the double-crosslinked hydrogel fabricated with PDA and PEGDA exhibits high G' and low G''. The incorporation of recoverable non-covalent interactions including π–π stacking and hydrogen bonding enables efficient energy dissipation through bond rupture during deformation. This mechanism prevents crack propagation during stretching while maintaining dimensional stability, allowing the gel to resist both deformation under high formation pressures and structural failure under mechanical stress.

3.3. Micromorphology and structure of DSDG

The microstructure of DSDG was examined using a field-emission SEM. Fig. 14 compares the network architectures of PAM-PEGDA and DSDG at identical 100 × magnification. As shown in Fig. 14(a), the PAM-PEGDA hydrogel exhibits a loose network

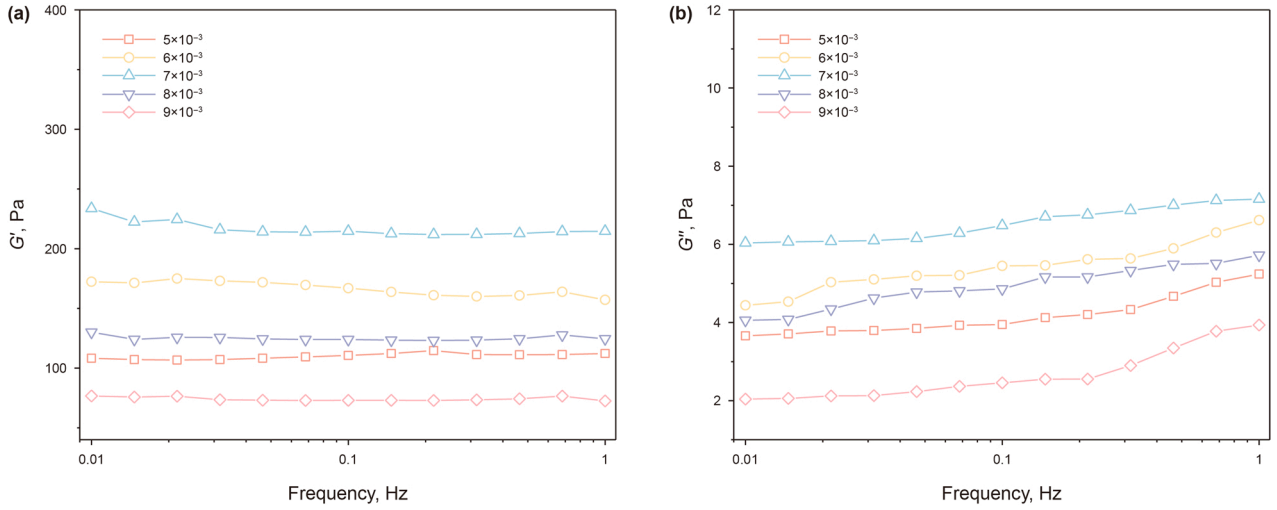

Fig. 13. G' (**a**) and G'' (**b**) of the prepared DSDG with different DA/AM mass ratios.

structure with low crosslinking density. In contrast, DSDG with DA/AM mass ratios of (5–9) × 10^{-3} display substantially denser crosslinked networks under the same magnification, as shown in Fig. 14(b)–(d). Within the DA/AM mass ratio range of (5–7) × 10^{-3}, the crosslinking density increases proportionally with DA/AM mass ratio, attributed to enhanced covalent and non-covalent interactions. Conversely, at higher DA/AM mass ratio of 9 × 10^{-3}, crosslinking density inversely correlates with DA/AM content due to excessive free DA monomers disrupting network formation. At a DA/AM mass ratio of 7 × 10^{-3}, DSDG exhibits the most compact network architecture. SEM imaging demonstrates enhanced crosslinking density from the PDA-PEGDA dual-crosslinked structure and concurrently verifies the inhibition effect of excess free DA monomers on the radical polymerization at the higher ratio (9 × 10^{-3}). Rheological results corroborate this trend: DSDG achieves maximum G' and optimal mechanical properties at 7 × 10^{-3}, with the minimum G' at 9 × 10^{-3}.

The possible double-crosslinked structures between PDA, PEGDA, and PAM were investigated by analyzing the FTIR spectra. Fig. 15 presents the FTIR spectra of PAM-PEGDA hydrogel, pure PDA, and DSDG. The PAM-PEGDA hydrogel exhibits an absorption band at 1120 cm^{-1} (C–O–C stretching vibrations). Notably, no characteristic C=C absorption peak at 1630–1650 cm^{-1} was detected, confirming complete opening and participation of the double bonds in PEGDA during crosslinking. The disappearance of C=C peaks and emergence of C–O–C peaks validate the occurrence of PAM-PEGDA crosslinking. In comparison to PAM-PEGDA hydrogel and pure PDA, the FTIR spectrum of DSDG exhibits a new peak at 1320 cm^{-1}, corresponding to C–N stretching vibrations in phenylamine groups. The presence of this band confirms interactions between the $–NH_2$ groups of PAM and the catechol groups of PDA. Furthermore, a distinct peak emerges at 1665 cm^{-1}, assigned to C=N stretching vibrations of Schiff base adducts, verifying covalent crosslinking between PAM and PDA. Notably, the absence of C=C characteristic absorption peaks within the 1630–1650 cm^{-1} range in DSDG definitively validates its double–crosslinked architecture (Wu et al., 2011).

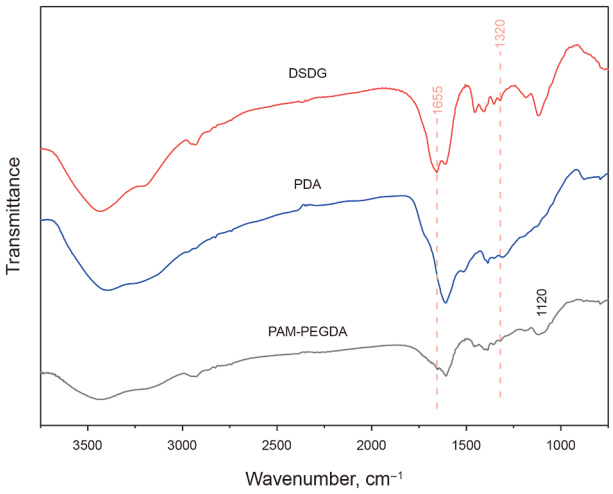

Fig. 15. The FTIR spectra of PAM-PEGDA hydrogels, PDA and DSDG.

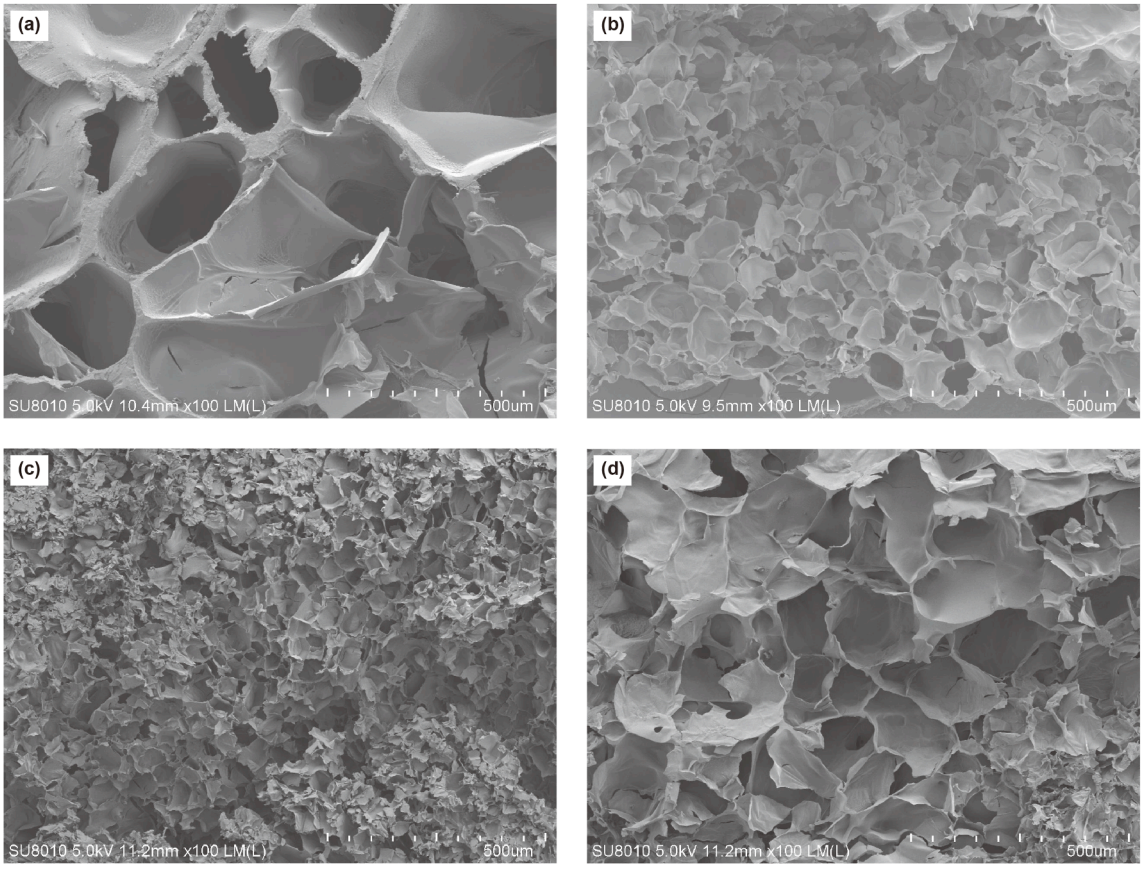

Fig. 14. SEM images of hydrogels with different DA/AM mass ratios: (**a**) 0, (**b**) 5 × 10^{-3}, (**c**) 7 × 10^{-3}, (**d**) 9 × 10^{-3}.

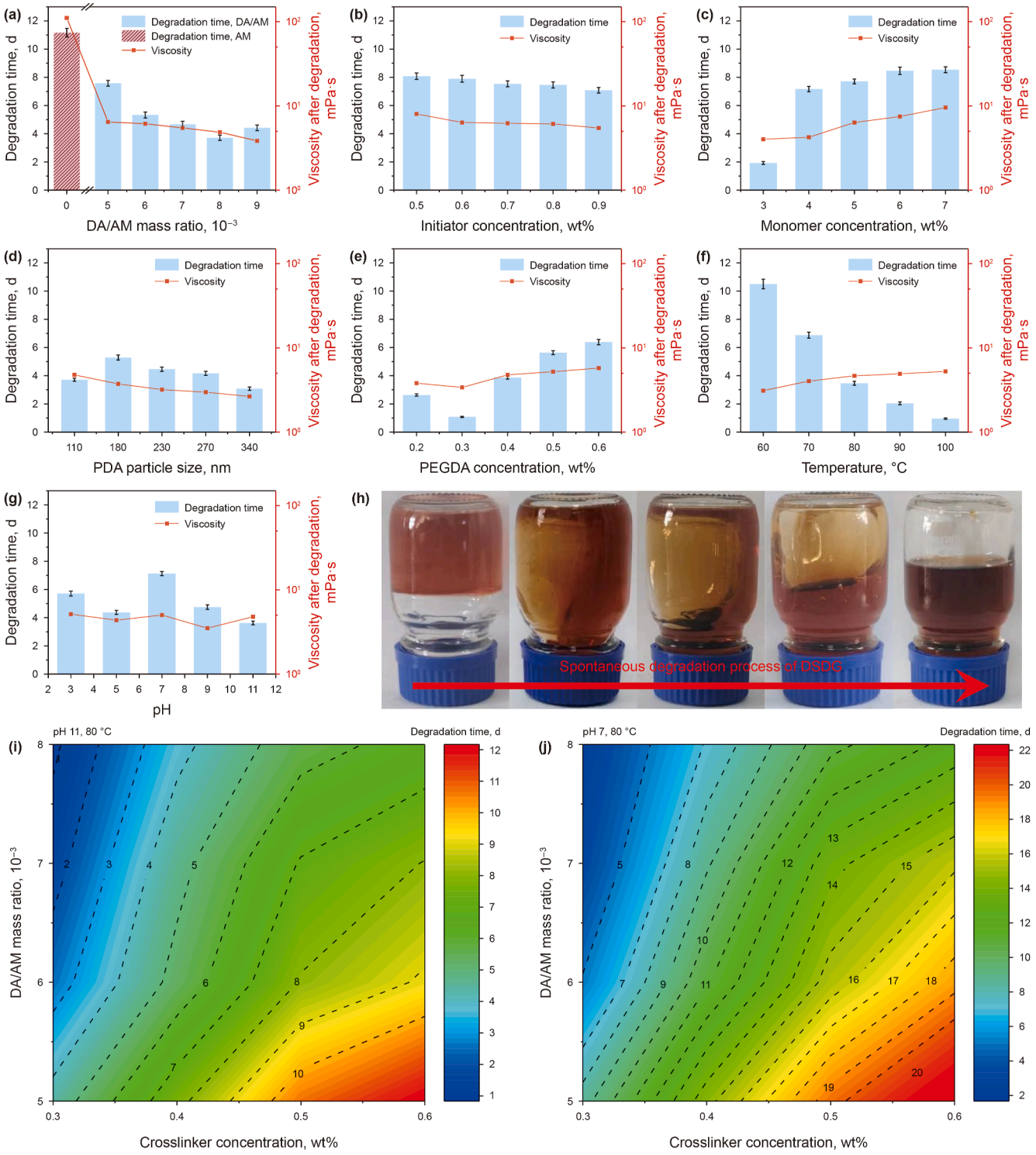

Fig. 16. Spontaneous degradation time and viscosity after degradation of DSDG under different conditions: (**a**) DA/AM mass ratio, (**b**) initiator concentration, (**c**) monomer concentration, (**d**) PDA particle size, (**e**) PEGDA concentration, (**f**) temperature, (**g**) pH. (**h**) Images of the spontaneous degradation process of DSDG. Distribution of spontaneous degradation time of gel under different PEGDA concentration and DA/AM mass ratio: (**i**) pH 11, (**j**) pH 7.

3.4. Spontaneous degradation

The degradation time and post-degradation viscosity of DSDG were systematically investigated under fixed conditions at 80 °C and pH 11. Fig. 16(a) illustrates the relationship between DA/AM mass ratio and degradation behavior. Increasing the DA/AM mass ratio initially shortened degradation time but extended it at higher ratios, while post-degradation viscosity consistently decreased. These experiments were conducted at fixed 5 wt% AM, 0.4 wt% PEGDA, and 0.6 wt% KPS. The observed trends arise from competing mechanisms. Elevated DA/AM mass ratios enhance the proportion of PDA-mediated crosslinks and intensify the

suppression of PEGDA crosslinking due to the increased reducing power of the system, accelerating network disintegration upon PDA degradation. Simultaneously, complex multi-crosslinked architectures formed at higher DA/AM mass ratios necessitate additional degradation pathways, prolonging the process. Reduced polymer molecular weight at higher DA/AM mass ratios, coupled with PDA hydrophilicity, promotes hydrogen bonding with water molecules, enhancing polymer dispersion and reducing intermolecular interactions, thereby lowering post-degradation viscosity.

Higher KPS concentrations reduce polymer molecular weight by generating shorter chain segments that facilitate gel degradation. However, when the initiator concentration exceeds 0.6 wt%, the rate of degradation time reduction diminishes progressively, as polymer chain lengths approach their minimum achievable values under these conditions. This trend is corroborated by the post-degradation viscosity data presented in Fig. 16(b). As shown in Fig. 16(b), increasing initiator concentration decreases DSDG degradation time while reducing post-degradation viscosity. These experiments were conducted using fixed parameters of 5 wt% AM, 0.4 wt% PEGDA, and a DA/AM mass ratio of 5×10^{-3}. The inverse correlation between initiator concentration and viscosity arises from the formation of shorter polymer chains, which exhibit weaker intermolecular interactions and enhanced water dispersibility.

Fig. 16(c) demonstrates the influence of monomer concentration on degradation time and post-degradation viscosity. Using fixed parameters of 0.4 wt% PEGDA, 0.6 wt% KPS, and a DA/AM mass ratio of 8×10^{-3}, DSDG degradation time increased with AM concentration, while post-degradation viscosity increased proportionally with monomer content. Elevated AM concentrations increase polymer chain length. Concurrently, the formation of a denser three-dimensional network reduces water molecule accessibility within the structure, retarding hydrolysis of PEGDA and PDA. These factors collectively contribute to prolonged gel degradation time and increased post-degradation viscosity.

Fig. 16(d) summarizes the influence of PDA particle size on gel degradation time and post-degradation viscosity under fixed experimental conditions of 5 wt% AM, 0.4 wt% PEGDA, 0.6 wt% KPS, and a DA/AM mass ratio of 8×10^{-3}. PDA particle size correlates positively with pre-polymerization stirring duration. Prolonged stirring increases PDA particle size while reducing free DA monomer content and overall reducibility, accompanied by a decrease in specific surface area. These changes diminish the density of reactive surface sites on PDA particles, weakening their inhibitory effect on PEGDA crosslinking and lowering the proportion of PDA-mediated crosslinks within the gel network, thereby impeding degradation. However, extended stirring oxidizes a significant fraction of catechol groups, reducing gel strength and adhesion. The resulting weaker, looser network exhibits lower stability and faster degradation, yielding lower post-degradation viscosity. Consequently, degradation time increases with PDA particle size in the 110–180 nm range but inversely correlates with size in the 230–340 nm range. Post-degradation viscosity consistently decreases with larger PDA particle sizes across the tested range of 110–340 nm.

Fig. 16(e) illustrates the influence of PEGDA concentration on degradation time and post-degradation viscosity. These experiments were conducted using fixed parameters of 5 wt% AM, 0.6 wt% KPS, and a DA/AM mass ratio of 8×10^{-3}. At low PEGDA concentrations below 0.3 wt%, prolonged crosslinking resulted in near-complete PDA degradation, diminishing its role in network integrity and polymerization inhibition, thereby extending degradation time and increasing viscosity. Conversely, higher PEGDA concentrations (> 0.3 wt%) introduced additional ester-based crosslinks between PAM chains. Since PEGDA degrades slower than PDA, its increased crosslink density reduced the relative contribution of PDA-mediated crosslinks, delaying structural disintegration and elevating post-degradation viscosity.

The effects of external factors such as temperature and pH on degradation time were investigated under fixed experimental parameters of 5 wt% AM, 0.4 wt% PEGDA, 0.6 wt% KPS, and a DA/AM mass ratio of 8×10^{-3}. Fig. 16(f) illustrates the temperature-dependent degradation behavior. Higher temperatures accelerated gel degradation rates due to increased thermal energy facilitating the activation energy required for ester bond and PDA degradation. Additionally, elevated temperatures promoted rearrangement or repolymerization of degradation products while intensifying entanglement among degraded polymer chains, thereby increasing post-degradation viscosity.

Fig. 16(g) demonstrates the pH-dependent degradation behavior of DSDG. Ester bond hydrolysis occurs faster in alkaline conditions than in acidic environments, while PDA degrades more rapidly under strong alkalinity. Consequently, DSDG exhibits shorter degradation times in alkaline media, with degradation duration decreasing as pH increases. Conversely, the degradation time increases under acidic conditions due to protonation of PDA surface amino groups ($-NH_2$ to $-NH_3^+$) at low pH, which stabilizes the structure and retards degradation. At neutral conditions, PDA remains nearly undegraded, and ester bond hydrolysis is significantly slower compared to acidic/alkaline conditions, resulting in the longest degradation time. Notably, post-degradation viscosity remains low across all pH conditions.

Fig. 16(h) displays the spontaneous degradation process of DSDG prepared with the standard formulation using 5 wt% AM, 0.4 wt% PEGDA, 0.6 wt% KPS, and a DA/AM mass ratio of 8×10^{-3} at pH 11 and 80 °C, demonstrating progressive structural disintegration rather than instantaneous failure. Further parametric optimization of PEGDA crosslinker concentration and DA/AM mass ratio was conducted to evaluate their impact on degradation time. Experimental data were used to construct Fig. 16(i) and (j), confirming that DSDG achieves controllable self-degradation within 1–20 d by adjusting the PEGDA/AM/DA formulation ratios and pH.

The PDA component within the DSDG network undergoes rapid degradation under acidic or alkaline conditions via hydrolysis of its dynamic covalent bonds, outpacing the degradation of the PEGDA cross-linker. This compromises the structural integrity of the gel network. Subsequently, residual PEGDA cross-linking sites self-degrade through spontaneous ester-bond hydrolysis in the bulk, leading to complete network disintegration. The structural damage initiated by PDA degradation accelerates this process.

3.5. Gel temporary plugging performance

The pressure-bearing capacity of DSDG in wellbores and matrix cores was evaluated under fixed formulation parameters of pH 11, 5 wt% AM, 0.4 wt% PEGDA, and 0.6 wt% KPS. The influence of DA/AM mass ratio on pressure resistance was investigated at 80 °C using a simulated wellbore model, with results summarized in Fig. 17. The maximum pressure-bearing capacity exhibited a peak value, increasing with DA/AM mass ratio up to 7×10^{-3}, beyond which performance declined. Below DA/AM ratios of 7×10^{-3}, rising ratios progressively increased G' and crosslinking density via abundant PDA catechol groups, which enhanced interfacial adhesion across diverse substrates and network integrity. This resulted in a pressure-bearing capacity of 1.25 MPa/m at the optimal DA/AM mass ratio of 7×10^{-3}. Above 7×10^{-3} DA/AM, excessive reducibility of the gel solution suppressed network formation, reducing crosslinking density and G'. Gels with diminished G' underwent deformation under stress, leading to fluid leakage along wellbore walls and eventual plugging failure. Despite this, at DA/

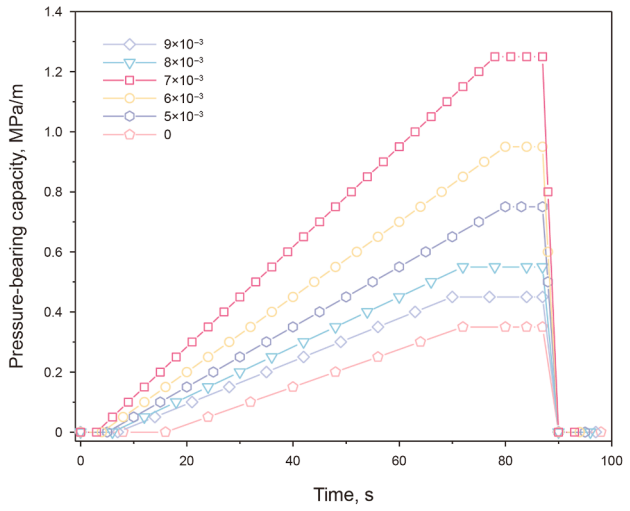

Fig. 17. Pressure-bearing capacity curves of gel in simulated wellbore at varying DA/AM mass ratios.

AM ratio of 9×10^{-3}, DSDG retained a pressure-bearing capacity of 0.45 MPa/m, outperforming the PDA-free control system. The inferior performance of the control system stemmed from reliance on weak physical adsorption for substrate bonding and its looser network structure with lower crosslinking density compared to double-crosslinked DSDG.

Core flooding experiments using homogeneous sandstone cores were conducted to investigate the effects of DA/AM mass ratio and permeability on the plugging efficiency of the gel system. The experiments were performed with fixed parameters of 5 wt% AM, 0.4 wt% PEGDA, 0.6 wt% KPS, pH 11, and 80 °C. Cores 1–3 were utilized to analyze permeability effects, while Cores 4–7 evaluated the influence of DA/AM mass ratio. Fig. 18(a) illustrates the pressure-bearing capacity of the gel with the DA/AM mass ratio of 8×10^{-3} across varying permeabilities. During the initial waterflooding stage, core injection pressure remained low. The injection pressure gradually increased as the gel viscosity rose during gelation. The 5 mD homogeneous core recorded the highest injection pressure of 0.61 MPa at 2 PV. Post-gelation waterflooding revealed gel breakthrough followed by propagation within the core. After the first droplet appeared at the core holder outlet, the plugging pressure continued to rise and stabilized with prolonged water injection. This behavior is attributed to gel elasticity and adhesion, which allowed it to adapt to pore channel geometries under pressure, forming stable plugs at pore throats despite deformation and propagation. While gel propagation was more pronounced in the 50 mD core, which resulted in weaker plugging performance, the 5 mD core with denser pore structures facilitated stable plug formation. As shown in Fig. 18(a), the gel demonstrated optimal plugging efficiency in the 5 mD core, achieving an initiation pressure gradient of 119 MPa/m and a breakthrough pressure gradient of 137.2 MPa/m. In contrast, the 50 mD core exhibited gel significant propagation, with initiation and breakthrough pressure gradients of 34.6 and 86.6 MPa/m, respectively.

Fig. 18(b) illustrates the influence of DA/AM mass ratio on pressure-bearing performance in homogeneous cores with identical permeability (10 mD). During the initial waterflooding stage, pressure differentials ranged from 0.09 to 0.17 MPa. After gel injection began, systems with DA/AM ratios of (5–9) $\times 10^{-3}$ exhibited slower pressure rise rates, reaching a maximum pressure of 0.54 MPa after 2 PV injection. In contrast, the DA-free control system achieved a significantly higher pressure of 1.52 MPa under the same conditions, highlighting the improved injectability of DA-modified gels. This enhancement stems from strong DA reducibility, which delays gelation by suppressing polymerization, thereby extending the low-viscosity phase critical for placement. Post-gelation waterflooding revealed propagation phenomena in DA-containing gels after breakthrough, whereas the control system stabilized rapidly without propagation due to the low mechanical strength of pure PAM gels, which fractured under shear stress. The DA/AM ratio of 7×10^{-3} demonstrated optimal propagation behavior, yielding an initiation pressure gradient of 110.2 MPa/m and a breakthrough pressure gradient of 184.6 MPa/m. At suboptimal ratios of 5×10^{-3} and 9×10^{-3}, reduced elastic modulus increased gel deformability under stress, leading to premature plugging failure. Despite this, these systems still outperformed the control, achieving initiation pressures of 79.6 and 68.0 MPa/m, with breakthrough pressures of 154.8 and 119.4 MPa/m, respectively. The control system exhibited markedly inferior performance, with initiation and breakthrough pressures of only 55.6 and 61.6 MPa/m, underscoring the superior sealing potential of DSDG in porous media dominated by matrix flow.

The formation protection performance of temporary plugging agents is critical for effective plugging removal and permeability restoration post-degradation. Artificial sandstone cores with

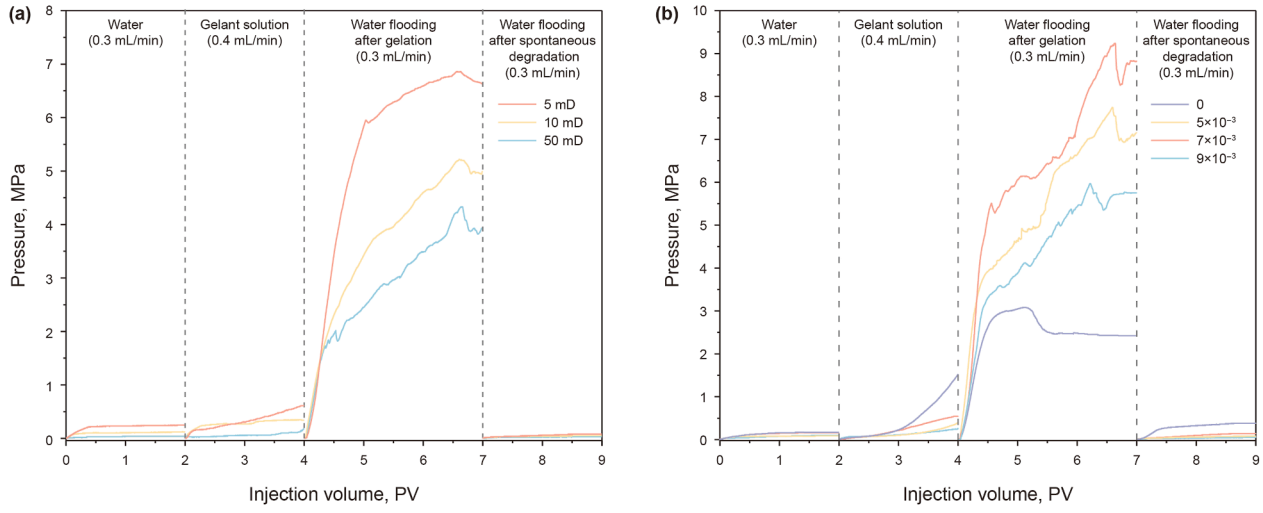

Fig. 18. The injection pressure curve of core flooding experiment: (**a**) different permeabilities, (**b**) different DA/AM mass ratios.

Table 2
Plugging capacity of gel system in homogenous cores.

Number	Core permeability, mD	DA/AM mass ratio	Pressure before injection of gel, MPa	Injection pressure of gel solution, MPa	Starting pressure gradient, MPa/m	Breakthrough pressure gradient, MPa/m	Pressure after spontaneous degradation, MPa
1	4.97	8×10^{-3}	0.04	0.61	119	137.2	0.03
2	10.85	8×10^{-3}	0.12	0.34	59.4	104.2	0.05
3	49.72	8×10^{-3}	0.25	0.18	34.6	86.6	0.10
4	9.91	5×10^{-3}	0.09	0.54	79.6	154.8	0.08
5	11.01	7×10^{-3}	0.16	0.40	110.2	184.6	0.14
6	9.76	9×10^{-3}	0.10	0.26	68.0	119.4	0.06
7	10.42	0	0.17	1.52	55.6	61.6	0.38

permeabilities of 5–50 mD were used to evaluate the formation protection efficacy of different formulations (Table 2) under pH 11 and 80 °C. All formulations maintained fixed parameters including 5 wt% AM monomer, 0.4 wt% PEGDA crosslinker, and 0.6 wt% KPS initiator. Pre-injection and post-degradation waterflooding pressure curves are shown in Fig. 18, with specific pressure values listed in Table 2. Table 2 reveals that post-degradation waterflooding pressures of DSDG in 5–50 mD cores did not exceed pre-injection baselines. This outcome is attributed to the complete degradation of DSDG within the core matrix, which minimized formation damage, combined with pore network restructuring induced by gel compression and subsequent release during plugging–degradation cycles. The synergistic interplay of these processes merged or enlarged micropores, enhanced pore connectivity, and ultimately reduced post-degradation waterflooding pressures. In contrast, DA-free control gels exhibited significantly higher post-degradation pressures, indicating severe formation damage. These results confirm that the self-degrading residues of DSDG were fully displaceable from matrix cores, preserving formation permeability and productivity with exceptional formation protection capabilities.

4. Conclusions

This study developed DSDG as a liquid temporary plugging agent for low temperature reservoirs. The synergistic degradation of DSDG, driven by hydrolysis of ester groups in the unstable crosslinker PEGDA and pH-sensitive degradation of PDA, enabled controllable self-degradation within 1–20 d, meeting the temporary plugging duration requirements for fracturing, drilling, and well intervention operations. The abundant catechol groups, π–π stacking interactions, and hydrogen bonds in PDA endowed the hydrogel with superior mechanical strength and adhesion properties, which enabled robust sealing under downhole stresses. Rheological tests and compressive experiments demonstrated that the post-gelation viscosity of DSDG exceeded 1.0×10^5 mPa·s. In homogeneous cores with permeabilities of 5–50 mD, DSDG achieved initiation and breakthrough pressure gradients of 34.6–119 and 86.6–184.6 MPa/m, respectively. In simulated wellbore with an inner diameter of 120 mm, the pressure-bearing capacity reached 1.25 MPa/m. Free DA monomers inhibited AM polymerization, shortening PAM chain lengths to avoid premature gelation and reducing post-degradation solution viscosity. The optimized DSDG formulation comprised 4–8 wt% AM monomer, 0.5–0.9 wt% KPS initiator, and 0.2–0.6 wt% PEGDA crosslinker, with a DA/AM mass ratio of $(5–8) \times 10^{-3}$. At 60–80 °C, DSDG transitions from liquid to quasi-solid gel within 30–180 min, with > 80% of the gelation process occurring in a low viscosity phase conducive to pumpable injection. Post-degradation viscosity was below 10 mPa·s, and the degraded fluid was fully displaceable from the core matrix, resulting in minimal formation damage.

CRediT authorship contribution statement

Tai-Heng Yin: Writing – original draft, Project administration, Funding acquisition, Conceptualization. **Yu-Meng Zhu:** Writing – original draft, Investigation, Data curation. **Yu-Qi Yang:** Writing – review & editing, Resources, Funding acquisition, Data curation. **Shen-Gen Chen:** Validation. **Ji-Rui Chen:** Formal analysis. **Yuan-Yuan Lu:** Investigation. **Han-Yu Guo:** Methodology. **Tao Wan:** Resources. **Jian Liu:** Supervision.

Declaration of interests

The authors declare that they have no known competing financial interests or personal relationships that could have appeared to influence the work reported in this paper.

Acknowledgments

This work was supported by the Research Foundation of China University of Petroleum–Beijing at Karamay (XQZX20250027), the Karamay Innovative Environment Construction Plan (Innovative Talents) Project (2025DB0047), the National Natural Science Foundation of China (52574069, 52504048), the PetroChina Innovation Foundation (2024DQ02-0148), the Tianshan Talent Project of Xinjiang Uyghur Autonomous Region (2022TSYCCX0057), the Xinjiang Tianshan Innovation Team (2022TSYCTD0002), the Xinjiang Uygur Autonomous Region Key Research and Development Project (2022B01058-2), and the Xinjiang Uyghur Autonomous Region "One Case One Discussion" Strategic Talent Research Team Introduction Project (XZT3-3).

Appendix A. Supplementary data

Supplementary data to this article can be found online at https://doi.org/10.1016/j.petsci.2025.11.025.

References

Bai, Y.R., Dai, L.Y., Sun, J.S., et al., 2022. Plugging performance and mechanism of an oil-absorbing gel for lost circulation control while drilling in fractured formations. Pet. Sci. 19 (6), 2941–2958. https://doi.org/10.1016/j.petsci.2022.08.004.

Bai, Y.R., Zhu, Y.C., Sun, J.S., et al., 2023. High stability polymer gel for lost circulation control when drilling in fractured oil and gas formations. Geoenergy Sci. Eng. 225, 211722. https://doi.org/10.1016/j.geoen.2023.211722.

Chen, S.L., Zhou, T.T., Wu, H., et al., 2017. Embedding molecular amine functionalized polydopamine submicroparticles into polymeric membrane for carbon capture. Ind. Eng. Chem. Res. 56, 8103–8110. https://doi.org/10.1021/acs.iecr.7b01546.

Chen, X., Yang, W.D., Zhang, J.J., et al., 2021. Alkalinity triggered the degradation of polydopamine nanoparticles. Polym. Bull. 78 (8), 4439–4452. https://doi.org/10.1007/s00289-020-03312-2.

Deng, Z.W., Shang, B., Peng, B., 2018. Polydopamine based colloidal materials: Synthesis and applications. Chem. Rec. 18 (4), 410–432. https://doi.org/10.1002/tcr.201700051.

Du, L.L., Liao, R.X., Zhang, H.J., et al., 2022. Redox-activity of polydopamine for ultrafast preparation of self-healing and adhesive hydrogels. Colloids Surf. B Biointerfaces 214, 112469. https://doi.org/10.1016/j.colsurfb.2022.112469.
Du, X.Y., Feng, S.B., Lu, H.Y., et al., 2023. Evaluation of supramolecular gel properties and its application in drilling fluid plugging. Processes 11 (9), 2749. https://doi.org/10.3390/pr11092749.
Guo, Z.Y., Zhang, Z.Z., Zhang, N., et al., 2022. A Mg^{2+}/polydopamine composite hydrogel for the acceleration of infected wound healing. Bioact. Mater. 15, 203–213. https://doi.org/10.1016/j.bioactmat.2021.11.036.
Han, L., Yan, L.W., Wang, K.F., et al., 2017. Tough, self-healable and tissue-adhesive hydrogel with tunable multifunctionality. NPG Asia Mater. 9 (4), e372. https://doi.org/10.1038/am.2017.33.
He, J.Y., Okere, C.J., Su, G.D., et al., 2021. Formation damage mitigation mechanism for coalbed methane wells via refracturing with fuzzy-ball fluid as temporary blocking agents. J. Nat. Gas Sci. Eng. 90, 103956. https://doi.org/10.1016/j.jngse.2021.103956.
Ji, R.J., Yu, X.R., Yang, H., et al., 2024. Preparation and degradable mechanism of self-breaking gel valve for underbalanced drilling. Geoenergy Sci. Eng. 235, 212705. https://doi.org/10.1016/j.geoen.2024.212705.
Jia, H., Yang, X.Y., Zhao, J.Z., 2019. Development of a novel in-situ-generated foamed gel as temporary plugging agent used for well workover: Affecting factors and working performance. SPE J. 24 (4), 1757–1776. https://doi.org/10.2118/194215-PA.
Jia, H., Chen, H., Zhao, J.Z., 2020. Development of a highly elastic composite gel through novel intercalated crosslinking method for wellbore temporary plugging in high-temperature reservoirs. SPE J. 25 (6), 2853–2866. https://doi.org/10.2118/201090-PA.
Jia, H., Kang, Z., Li, Z.J., 2022. The potential of ultrahigh strength gel through novel multistage reinforcement method for sealing operations in medium to ultra-low temperature reservoirs. SPE J. 27 (4), 2145–2160. https://doi.org/10.2118/209602-PA.
Jia, H., Li, P.W., Zhang, Y.F., 2024. Polymer gel for water shutoff in complex oil and gas reservoirs: Mechanisms, simulation, and decision-making. SPE J. 29 (1), 243–259. https://doi.org/10.2118/217457-PA.
Khan, N., Pu, J.Y., Pu, C.S., et al., 2019. Experimental and mechanism study: Partially hydrolyzed polyacrylamide gel degradation and deplugging via ultrasonic waves and chemical agents. Ultrason. Sonochem. 56, 350–360. https://doi.org/10.1016/j.ultsonch.2019.04.018.
Li, J.B., Luo, Z.F., Fu, H.R., et al., 2024. Research and application of the low-damage temperature-controlled phase change temporary plugging agent. Geoenergy Sci. Eng. 241, 213122. https://doi.org/10.1016/j.geoen.2024.213122.
Li, L.Y., Lu, F.X., W, C., et al., 2018. Flexible double-cross-linked cellulose-based hydrogel and aerogel membrane for supercapacitor separator. J. Mater. Chem. A 6 (47), 24468–24478. https://doi.org/10.1039/C8TA07751G.
Li, S.L., Zhou, H.W., Li, Y.F., et al., 2022. Mussel-inspired self-adhesive hydrogels by conducting free radical polymerization in both aqueous phase and micelle phase and their applications in flexible sensors. J. Colloid Interface Sci. 607, 431–439. https://doi.org/10.1016/j.jcis.2021.08.205.
Lin, J.H., Yu, C.J., Yang, Y.C., et al., 2015. Formation of fluorescent polydopamine dots from hydroxyl radical-induced degradation of polydopamine nanoparticles. Phys. Chem. Chem. Phys. 17, 15124–15130. https://doi.org/10.1039/c5cp00932d.
Liu, C., Zou, H.J., Wang, Y.G., et al., 2024. Degradation behavior and mechanism of P(AM/AA/AMPS)@PLA core-shell self-degrading temporary plugging agent. J. Mol. Liq. 393, 123656. https://doi.org/10.1016/j.molliq.2023.123656.
Liu, C.Y., Huang, C.J., 2016. Functionalization of polydopamine via the Aza-Michael reaction for antimicrobial interfaces. Langmuir 32, 5019–5028. https://doi.org/10.1021/acs.langmuir.6b00990.
Liu, J.R., Sheng, J.J., Emadibaladehi, H., et al., 2021. Experimental study of the stimulating mechanism of shut-in after hydraulic fracturing in unconventional oil reservoirs. Fuel 300, 120982. https://doi.org/10.1016/j.fuel.2021.120982.
Mandal, M., Kumar, R.P., Ojha, K., 2024. Impact assessment of polymer, cross-linker, and nanoparticles on gelation kinetics and properties of silica nanocomposite hydrogel for water shut-off treatment in harsh reservoir conditions. J. Mol. Liq. 411, 125746. https://doi.org/10.1016/j.molliq.2024.125746.
Peng, L., Liang, Y.F., Yue, J.L., et al., 2023. Dramatic improvement in the mechanical properties of polydopamine/polyacrylamide hydrogel mediated human amniotic membrane. RSC Adv. 13, 3635–3642. https://doi.org/10.1039/D2RA07622E.
Wang, Y., Liu, D.J., Liao, R.Q., et al., 2022. Study of adhesive self-degrading gel for wellbore sealing. Colloids Surf. 651, 129567. https://doi.org/10.1016/j.colsurfa.2022.129567.
Wu, J.J., Zhang, L., Wang, Y.X., et al., 2011. Mussel-inspired chemistry for robust and surface-modifiable multilayer films. Langmuir 27, 13684–13691. https://doi.org/10.1021/la2027237.
Wu, M.X., Hong, C.Y., Shen, C.J., et al., 2023. Polydopamine nanomaterials and their potential applications in the treatment of autoimmune diseases. Drug Deliv. 30 (1), 2289846. https://doi.org/10.1080/10717544.2023.2289846.
Xu, Y.T., Hu, J.F., Hu, J.J., et al., 2023. Bioinspired polydopamine hydrogels: Strategies and applications. Prog. Polym. Sci. 146, 101740. https://doi.org/10.1016/j.progpolymsci.2023.101740.
Yang, Z.T., Ni, R.X., Yang, Y., et al., 2024. Carboxymethyl cellulose-based supramolecular hydrogel with thermo-responsive gel-sol transition for temporary plugging of oil pipeline in hot work. Carbohydr. Polym. 324, 121556. https://doi.org/10.1016/j.carbpol.2023.121556.
Zhang, C., Wu, B.H., Zhou, Y.S., et al., 2020. Mussel-inspired hydrogels: From design principles to promising applications. Chem. Soc. Rev. 49 (11), 3605–3637. https://doi.org/10.1039/C9CS00849G.
Zhang, X., Deng, J.N., Yang, K., et al., 2022. High-strength and self-degradable sodium alginate/polyacrylamide preformed particle gels for conformance control to enhance oil recovery. Pet. Sci. 19 (6), 3149–3158. https://doi.org/10.1016/j.petsci.2022.06.012.
Zhao, Y., Bai, B.J., 2022. Selective penetration behavior of microgels in super-permeable channels and reservoir matrices. J. Petrol. Sci. Eng. 210, 109897. https://doi.org/10.1016/j.petrol.2021.109897.
Zhong, Y., Zhang, H., Feng, Y.H., et al., 2022. A composite temporary plugging technology for hydraulic fracture diverting treatment in gas shales: Using degradable particle/powder gels (DPGs) and proppants as temporary plugging agents. J. Petrol. Sci. Eng. 216, 110851. https://doi.org/10.1016/j.petrol.2022.110851.
Zhou, M., Muhammad, F., Zhang, Y.H., et al., 2025. Copper depletion-induced tumor cuproptosis. Chem. Sci. 16, 4226–4236. https://doi.org/10.1039/d4sc04712e.
Zhou, Q., Luo, Z.F., Fu, H.R., et al., 2025. Research and application progress of temporary plugging agent for acidification fracturing: A review. Geoenergy Sci. Eng. 247, 213600. https://doi.org/10.1016/j.geoen.2024.213600.
Zhu, D.Y., Hou, J.R., Wang, J.F., et al., 2018. Acid-alternating-base (AAB) technology for blockage removal and enhanced oil recovery in sandstone reservoirs. Fuel 215, 619–630. https://doi.org/10.1016/j.fuel.2017.11.090.
Zhu, D.Y., Hou, J.R., Wei, Q., et al., 2019. Development of a high-temperature-resistant polymer-gel system for conformance control in Jidong oil field. SPE Reservoir Eval. Eng. 22 (1), 100–109. https://doi.org/10.2118/186235-PA.
Zou, C.W., Dai, C.L., Liu, Y.F., et al., 2023. A novel self-degradable gel (SDG) as liquid temporary plugging agent for high-temperature reservoirs. J. Mol. Liq. 386, 122463. https://doi.org/10.1016/j.molliq.2023.122463.